Hyperthermal effects on nucleation and growth during low-energy ion deposition

Bart Degroote,* André Vantomme, Hugo Pattyn, and Koen Vanormelingen
Instituut voor Kern- en Stralingsfysica, Katholieke Universiteit Leuven, B-3001 Leuven, Belgium
(Received 29 November 2001; published 19 April 2002)

We have performed a systematic study on the influence of deposition energy on the morphology of submonolayer Co films grown on Ag(001) at ambient temperature. Co was deposited by low-energy ion deposition with a deposition energy between 5 and 30 eV. The island density, height, size distribution, and composition were studied using scanning tunneling microscopy. For increasing deposition energy, there is an increasing fraction of Co incorporated in the first monolayer of the surface. These Co atoms form surface-confined clusters, which can act as pinning centers for Co adatoms on top of the surface. These pinning centers promote an increase in island density compared to deposition with thermal particles ($\sim$0.1 eV). In addition, our experimental results indicate that both ion impact induced island fragmentation and dissociation play an important role during nucleation and growth. Island fragmentation is a mechanism that promotes an increase in island density compared to thermal deposition, whereas island dissociation promotes a decrease in island density.

DOI: 10.1103/PhysRevB.65.195401 PACS number(s): 79.20.Rf, 68.55.Ac, 68.37.Ef

I. INTRODUCTION

The physical properties of thin films grown with *hyperthermal* particles, i.e., involving energies above 1 eV, can differ significantly from films produced with *thermal* techniques, where particles have an energy of the order of 0.1 eV (see Refs. 1–24 in Ref. 1). There has been a considerable effort in the investigation of the atomic processes related to the impact of hyperthermal particles on a surface. These processes influence the morphology of a growing film, e.g., the island density, the island size distribution, and the growth mode [two dimensional (2D) or three dimensional (3D)] and can be divided into two groups. On the one hand there are mechanisms that affect the mobility of single atoms diffusing on the surface: transient mobility[2–6] and enhanced mobility due to direct or indirect ion impact.[7–10] On the other hand there are mechanisms related to the formation (or breaking up) of islands: nucleation at ion impact induced point defects,[11–13] the presence of pinning centers (this work), adatom sputtering,[7] island fragmentation, and island dissociation.[14–16]

Nucleation at ion impact induced adatom clusters has been proposed in several cases of metal homoepitaxy to explain the drastic increase in island density for hyperthermal techniques compared to thermal deposition. For ion-beam assisted deposition (IBAD) of Pt on Pt(111) at $T \geqslant 200$ K, the simultaneous bombardment with Ar^+ ions (400 eV and 4 keV) during deposition gives an increase of the island density by a factor of more than 10 (depending on ion energy and flux).[12] A similar effect was observed for ion-beam sputter deposition (IBSD) of Pt on Pt(111) at 300 K.[13] Compared to thermal deposition, the island density increases by a factor of 4–27, depending on the geometry of the deposition. Together with the sputtered atoms with a relatively low energy ($\pm$10 eV), there is a small fraction of energetic particles ($>$100 eV) impinging onto the substrate. In a small area around the impact of these particles, a number of adatom islands is created, which increases the number of nucleation centers.

With this drastic increase of the island density caused by nucleation at ion impact induced adatom clusters, the growth of a film can be improved significantly. For pulsed IBAD of Ag on Ag(111) and Cu on Cu(111), where a pulse of energetic particles is applied at the beginning of every new monolayer (ML), layer-by-layer growth was observed up to 7 ML whereas thermal deposition leads to 3D growth.[17]

For the cases of metal homoepitaxy described above, the nucleation at ion induced adatom clusters is a mechanism that explains the observed morphology quite well. The situation for heteroepitaxy, on the other hand, is more complicated, since one has to deal with aspects such as lattice misfit and intermixing. Despite many theoretical efforts,[7,14–16,18–20] there are only few experimental studies on metal heteroepitaxy with hyperthermal techniques that describe the changes in island density, size distribution, growth mode, etc. as a function of particle energy and compared to thermal deposition.[21] In our experiments this was done for submonolayer Co films grown on Ag(001) with low-energy ion deposition (LEID) in the energy range 5–30 eV. We have strong indications that the morphology is determined by island fragmentation and the presence of pinning centers on the one hand (causing an increase in island density) and by island dissociation on the other hand (causing a decrease in island density). Even though Ag adatoms are formed during deposition of Co for all energies used, we have no indication that nucleation at ion induced Ag adatoms causes an increase in island density.

II. EXPERIMENTAL

The Ag(001) substrates were prepared in ultrahigh vacuum (UHV) with molecular-beam epitaxy by growing a Cr buffer layer of 50 Å on a polished MgO(001) single crystal at 450 K, followed by an Ag film of 1000 Å grown at 300 K.[22,23] In order to obtain large atomically flat terraces ($>$500 Å) separated by monatomic steps, the film is annealed at 475 K for about 10 min. Submonolayer ^{59}Co films were grown with low-energy ion deposition. In LEID, the

ions are first accelerated to enable proper beam handling and mass separation and consequently decelerated for deposition on the substrate. Deposition is realized under UHV conditions ($<10^{-9}$ Torr) since the chamber is differentially pumped from the beam line. In our case, the mass separation occurs with a beam energy of 50 keV whereas the deposition energy can range from 0 to 200 eV. In order to calibrate the deposition energy, a grid is mounted on the sample holder. When the electrostatic potential of the grid is higher than the kinetic energy of the incoming ions, no ions can penetrate the grid. When this potential is lower, the ions penetrate, and their current can be measured. This method is suitable to assure reproducibility of the deposition energy with respect to a fixed reference potential (e.g., the potential where ions start to penetrate the grid). On the other hand, with this method it is difficult to determine the exact value of the spread in kinetic energy of the ions. As we experienced, the energy window from which the current through the grid increases from zero to maximum is very much dependent on the mesh of the grid.[23] This means that we can only give an upper limit for the energy spread. Using a grid of 0.76 mm we found a value of 7 V for the full width at half maximum (FWHM) using a Gaussian distribution. However, our experimental results indicate that this is an overestimation: the morphology changes drastically (and reproducibly) when the retarding potential is changed by an increment of 5 eV. This means that the FWHM of the energy spread is below 5 eV. We also mention that, in contrast to IBSD, for LEID we verified that there is no high-energy tail since the ions are extracted from a plasma under well-defined conditions. For details on the experimental setup we refer to Refs. 22 and 23. The Ag(001) substrate is at ambient temperature (300 K) during deposition. The $^{59}Co^{+}$ primary beam current is of the order of 200 nA for all experiments. This corresponds to a deposition rate $F=0.002$ Å/s as determined from quantitative scanning tunneling microscopy (STM) analysis of the Co island coverage (giving an error margin of about 10%). The Co ions hit the surface with an incident angle between 20° and 30° off normal.[23] After deposition, the sample is transported *in vacuo* to the UHV ($<5\times10^{-10}$ Torr) STM chamber.

III. RESULTS AND DISCUSSION

A. 5 eV

In Figs. 1(a) and 1(b) STM topographs are shown for deposition of Co on Ag(001) at 5 eV. Next to randomly distributed islands on the terraces, preferential nucleation is observed on the upper side of the Ag steps [see line profile in Fig. 1(c)]. Many islands are surrounded by a patch of ML height. The islands correspond to Co and the ML patches to Ag. This was concluded in a previous study concerning (thermal) codeposition experiments of Co and Ag, i.e., deposition Co and Ag atoms at the same time onto a Ag(001) substrate.[23] In that study we found that the nucleation and growth of Co islands is practically unaffected by the presence of Ag adatoms. These Ag adatoms only attach to already existing Co islands forming a ML patch [similar to the patches in Fig. 1(a)]. Co adatoms that attach to a Ag patch surrounding a Co island can migrate through the patch and become part of the island. In Fig. 1(d) a line profile is shown through such a Ag patch surrounding several Co islands.

The presence of Ag on the surface is also clear from the height histogram shown in Fig. 1(e): there is a peak at a height of 2 Å above terrace level. We note that in the histogram only large terrace areas with Co islands are taken into account (Ag steps of the substrate are not included). The substrate peak, which is set at a height of 0 nm, is not shown to get a better view on the tail of the histogram. We find that 63% of the Co coverage is in the first ML above terrace level, 29% in the second ML, and 8% in the third ML. A coverage of 0.42 ML of Co and 0.05 ML of Ag was found. The Ag coverage corresponds to the area under the peak at a height of 2 Å in the histogram. The same procedure was used in Ref. 23 for the codeposition experiments of Co and Ag on Ag(001). In fact, the morphology for 5 eV is very similar to the morphology observed for the codeposition experiments. However, since in LEID we only deposit Co atoms (one could say *monodeposition*), Ag adatoms can only originate from the exchange of an energetic Co atom with a Ag atom from the first surface layer. With molecular dynamics (MD) we simulated the energetic impact of a Co atom on a Ag(001) surface.[24] For a deposition energy of 5 eV we found that a large fraction of Co lands on top of the surface, becoming an adatom. There is also a minor fraction that penetrates into the surface. For deposition angles of 20° and 30°, respectively, 16(4)% and 9(3)% of Co atoms end up in the first surface layer. Each time such a Co atom arrives in a substitutional position in the first surface layer, a Ag atom becomes an adatom in the near vicinity of the impact. Therefore we can assume that the fraction of Ag observed on top of the surface is directly related to the fraction of Co in the first surface layer. The presence of 0.05 ML of Ag for the 5-eV experiment indicates that 11% of the Co ions [$0.05/(0.42+0.05)=0.11$] have ended up in the first surface layer of Ag. This corresponds very well with our MD calculations. We have already mentioned that the presence of these ion impact induced Ag adatoms does not affect the nucleation of the Co adatoms. This is different compared to IBAD and IBSD of Pt on Pt(111) where ion impact induced adatoms and clusters clearly act as nucleation centers.[12,13] This results in a considerable increase in island density compared to thermal deposition. Further investigation is needed to clarify this different behavior, e.g., its relation to homoepitaxy or heteroepitaxy and the difference between the close-packed (111) surface and the more open (001) surface of an fcc lattice.

There is also experimental evidence for the presence of Co in the first surface layer. Figure 2 shows an STM image with enhanced contrast on the Ag terrace level. One can clearly observe depressions in the terrace. The Co atoms that end up in the first surface layer after impact can diffuse and nucleate with other Co atoms in this layer. Instead of forming islands on top of the surface, they form clusters embedded in the surface also called *surface-confined clusters*. With STM these Co clusters are observed as depressions with respect to the Ag(001) terrace level, due to the smaller atomic radius of Co compared to Ag. Similar depressions have been observed for thermal deposition of Co on Ag(001) at 425 K.[25]

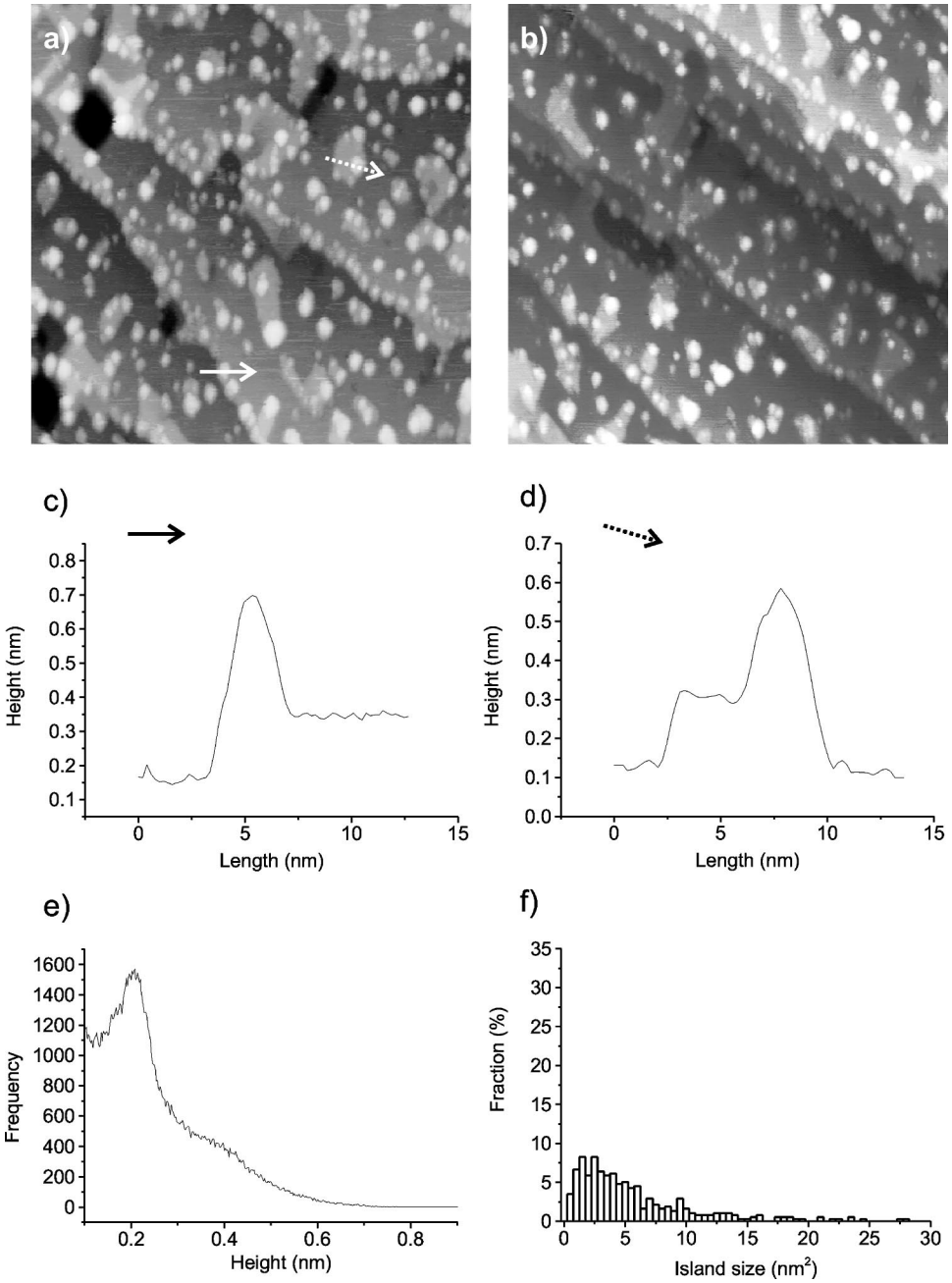

FIG. 1. An STM topograph (100×100 nm^2) of low-energy ion deposition of Co on Ag(001) at 5 eV in an area with large terraces (a), in an area with a high step density (b); a line profile taken along the solid white arrow (c), a line profile taken along the dotted white arrow (d); the height histogram taken from areas without Ag steps and with the terrace peak (not shown) at 0 nm (e) and the island size distribution (f) (the maximum value on the *y* axis is chosen to be 35% to allow better comparison between the different deposition energies).

From STM analysis on a large number of terraces, we found that the island density $n_{x,5\ \mathrm{eV}}=26(4)\times10^3$ islands/μm^2. Based on the results for thermal deposition at 300 K with $F=0.1$ Å/s, an island density of $n_{x,TD}=18(3)\times10^3$ islands/μm^2 is expected for a deposition rate of 0.002 Å/s (Ref. 23) using nucleation theory.[26] This means that also from the point of view of the island density, LEID with 5 eV and thermal deposition are comparable. The slightly higher value for the observed island density in the case of LEID is possibly due to the presence of surface-confined Co clusters. As shown in Fig. 2, many of the depressions are in the vicinity of an island, indicating that Co clusters in the first surface layer can act as pinning centers for Co adatoms, resulting in an increase of n_x. The Co island size distribution is shown in Fig. 1(f). The Ag patches were subtracted from the images retaining only Co islands. The size distribution is very similar to thermal deposition at 300 K.[23]

As pointed out above, at 5 eV we observe preferential nucleation of Co islands on the upper side of the Ag steps—also called *step decoration*. In areas with a high local step density, most of the Co atoms grow along the step edges [Fig. 1(b)]. Step decoration has only been observed for specific systems: Co on Cu(111),[27,28] Fe on Cu(111),[29,30] and now Co on Ag(001). Gomez *et al.* have proposed a mechanism to explain step decoration of Co on Cu(111): Co atoms incorporated at the step edges can act as pinning centers for Co adatoms on the upper terrace.[28] Based on the results of thermal deposition experiments[25] and molecular-dynamics simulations,[24] there are strong indications that a similar

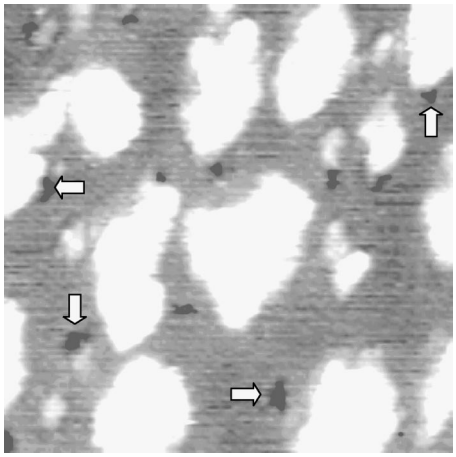

FIG. 2. An STM topograph (30×30 nm^2) of low-energy ion deposition of Co on Ag(001) at 5 eV with enhanced contrast on the Ag terrace level. The white arrows point at some of the depressions corresponding to surface-confined Co clusters.

mechanism is responsible for step decoration of Co on Ag(001).

In conclusion, the nucleation and growth of Co islands on top of the surface is hardly affected by the use of a hyperthermal deposition energy of 5 eV: the morphology is similar to the case of thermal deposition. However, there is a small fraction of Ag adatoms present on top of the surface and a small fraction of Co incorporated in the first surface layer.

B. 10 eV

The situation changes drastically after LEID of the same ion dose with 10 eV. We found an island density of 73(10) $\times10^3$ islands/μm^2 and a coverage of 0.52 ML of Co and 0.05 ML of Ag. The coverage at 10 eV is higher than at 5 eV (0.42 ML) due to the increased efficiency of the deceleration process for increasing deposition energy,[23] i.e., a larger fraction of ions is deposited on the same surface area. The islands are lower than in the case of 5 eV and, therefore, the surface area covered by the islands is larger: at 5 eV 26% of the total surface is covered by islands compared to 48% for 10 eV. As a consequence, island coalescence has to be taken into account. Since this is not opportune for our analysis of the island density, the 10-eV experiment was repeated with half the dose. This dose was used for the higher deposition energies as well.

In Fig. 3(a) an STM topograph is shown for a deposition energy of 10 eV with half the dose compared to 5 eV. The morphology is completely different than for 5-eV deposition. We obtain an island density of $87(20)\times10^3$ islands/μm^2, which is a factor of 3 higher than in the case of 5 eV. The shape of the height histogram is different as well. There is only a small Ag peak at 2 Å and the tail of the histogram is a lot shorter indicating that the islands are lower than for the 5-eV case. A coverage of 0.19 ML of Co and 0.03 ML of Ag is found. This corresponds to a fraction of 14% Co that has ended up in the first surface layer. This value is somewhat higher than for 5 eV, in agreement with our MD simulations.[24] From an analysis of the height of Co islands on top of the surface (using the histogram), we obtain a Co contribution of 89% in the first ML above the surface and 11% in the second ML.

In Fig. 3(b) an STM image is shown with enhanced contrast on the Ag terrace level. One can clearly observe depressions in the terrace. A considerable fraction of those depressions is in the near vicinity of an island, confirming that such clusters can act as a pinning center for Co adatoms on top of the surface. Due to this pinning mechanism, the increase of the buried cluster density will cause an increase of the island density. In order to investigate whether this explains the increase of the island density observed at 10 eV, we estimate the expected density of surface-confined clusters using nucleation theory.[26] Nucleation theory is developed to describe the formation of islands (on top of a surface) in two dimensions. Since the formation of clusters in the first surface layer is a 2D problem as well, the same equations can be used,

$$n_x = \eta(\theta,i)\left(\frac{D}{F}\right)^{-\chi}\exp\left(\frac{\chi E_i}{ikT}\right) \tag{1}$$

with n_x given as the number of islands per lattice site (in our case, the number of surface-confined clusters per lattice site). $\eta(\theta,i)$ contains the coverage (θ) dependence. The values for η as a function of θ and i in both the lattice approximation and the uniform depletion approximation can be found in Ref. 31 [Fig. 6(b)]. D is the diffusion coefficient and F is the deposition rate. E_i is the binding energy of a critical cluster with size i and χ is the scaling exponent. T is the temperature of the substrate.

In order to avoid confusion, we use $\tilde{n}_x$ for the density of surface-confined clusters whereas n_x is used for the density of islands on top of the surface. This is done for all parameters that can be both used for the surface and the subsurface case.

Only a fraction a, corresponding to 15–20 % of the deposited Co atoms, ends up in the first surface layer. This means that the effective arrival rate of Co atoms in the first surface layer is $\tilde{F}=a(0.002$ Å/s). If we assume a critical cluster size $\tilde{i}=1$ (which means that dimers are stable) and that the clusters are confined to only one layer, then $\tilde{E}_i=0$ (see Ref. 26) and $\tilde{\chi}=1/3$. The only remaining parameter in Eq. (1) is the diffusion coefficient for subsurface diffusion, $\tilde{D}$. Assuming an Arrhenius behavior, a diffusion coefficient can be expressed as a function of temperature T according to

$$D = D_0\exp\left(-\frac{\Delta E_d}{kT}\right), \tag{2}$$

where D_0 is the preexponential factor called the *diffusivity* and ΔE_d is the *activation energy* or the *diffusion barrier*.

In order to find a value for $\tilde{D}$, we first estimate the activation energy $\triangle\tilde{E}$ for subsurface diffusion. We use the experimental value $\tilde{n}_x=15(2)\times10^3/\mu$m^2 obtained for thermal deposition of Co at 425 K with $F=0.02$ Å/s.[25] Since in this case all Co atoms end up in the first surface layer $\tilde{F}=F$.

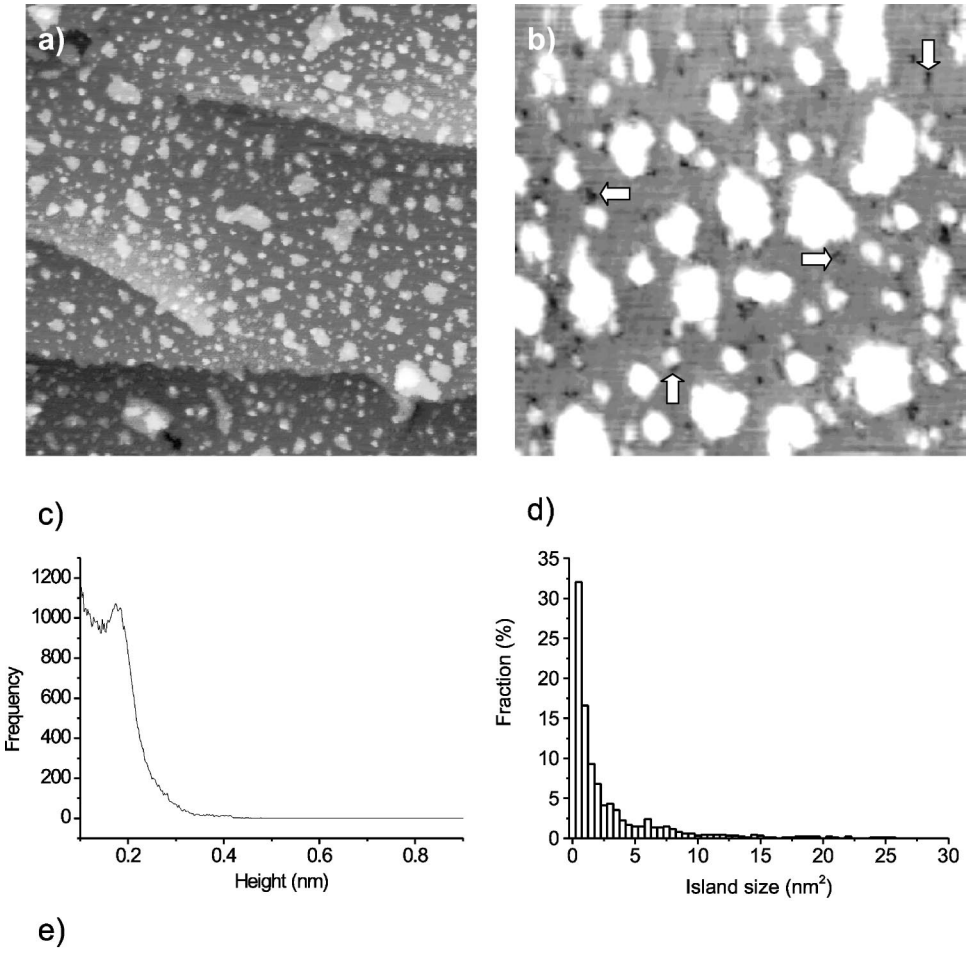

FIG. 3. An STM topograph (100×100 nm^2) of low-energy ion deposition of Co on Ag(001) at 10 eV (a); an STM topograph (30×30 nm^2) with enhanced contrast on the Ag terrace level, the white arrows point at some of the depressions (b), the height histogram taken from areas without Ag steps and with the terrace peak (not shown) at 0 nm (c), the island size distribution (d), and A side view of a Co cluster embedded in the first surface layer of Ag(001) (e). The black spheres correspond to Co atoms, the gray to the Ag positions taken by the Co atoms, and the white spheres to the Ag atoms.

Using Eq. (1) a diffusion coefficient $\tilde{D}=5(2)\times10^{-3}$ cm^2/s was found corresponding to a hopping freqency $\nu=6(3)\times10^4$ Hz. In studies on surface diffusion, it is common to assume that the attempt frequency $\nu_0=10^{12\pm1}$ Hz.[32–34] This gives an activation energy $\triangle\tilde{E}=0.7(1)$ eV. Using the same value for the diffusivity, a diffusion barrier for terrace hopping of $\triangle E=0.4(1)$ eV was found. As expected, this is lower than the activation energy for subsurface diffusion.

With $\tilde{\nu}_0=10^{12\pm1}$ Hz and $\triangle\tilde{E}=0.7(1)$ eV we can calculate the expected cluster density for a deposition rate $\tilde{F}=a(0.002$ Å /s) at 300 K. The surface-confined cluster density found for these values is $\tilde{n}_{x,10\text{ eV}}=5(2)\times10^4/\mu$m^2. In the case of 5 eV we find $\tilde{n}_{x,5\text{ eV}}=4(2)\times10^4/\mu$m^2 ($a_{5\text{ eV}}<a_{10\text{ eV}}$). Although deposition at 10 eV gives an increase of the density of pinning centers compared to 5 eV, the pinning mechanism alone cannot be responsible for an increase of the island density by a factor of 3 as observed in our experiments.

In the Introduction, we have already mentioned the mechanisms that possibly influence nucleation and growth when using hyperthermal particles: transient mobility, enhanced mobility due to direct or indirect ion impact, adatom sputtering, nucleation at ion impact induced point defects, the presence of pinning centers, island fragmentation, and island dissociation. Since transient mobility and enhanced mobility due to ion impact result in a decrease of the island density [Eq. (1)], these mechanisms cannot explain the increase of the island density for an increase of the deposition energy from 5 to 10 eV. In addition, the fraction of adatoms that is hit by an incoming ion is very small,[23] which means that both enhanced mobility due to ion impact and that due to adatom sputtering are of minor importance. In the case of Co on Ag(001), we can exclude nucleation at ion impact induced Ag adatoms: from codeposition experiments, we know that the Co island density is not influenced by the presence of Ag adatoms.[23] Island dissociation cannot explain the observed increase of the island density either: this mechanism causes

some islands to disappear during deposition resulting in a decrease of the island density. The only remaining mechanism that can explain the observed behavior of the island density is fragmentation: islands are not completely broken apart but only depleted at their edges. The Co adatoms that are created by the impact can form new islands or become a part of the already existing islands. Sillanpaä and Koponen modeled ion-beam assisted deposition by rate equations taking fragmentation into account.[14] They found that fragmentation causes the island density to increase and average island size to decrease.

In order to consider fragmentation as an acceptable explanation for the drastic increase of the island density, one has to prove that there is a sufficient number of Co ions hitting an island. The probability that ion k hits a Co island when arriving on the surface is equal to the island coverage θ_{island} at t_k, the time at which ion k arrives (note that for submonolayers $\theta_{island} \leqslant 1$),

$$P_{hit}(\text{ion } k) = \theta_{island}(t_k). \tag{3}$$

The island coverage increases linearly with the number of ions that is deposited within a certain area. For 1 ML, 1.2×10^7 ions have to be deposited [this is the number of adatom sites on 1 μm^2 of Ag(001)], and under the assumption of 2D growth $\theta_{island} = 1$. Subsequently, the total number of island hits N_{hits} on 1 μm^2 after deposition of n ions is

$$N_{hits} = \sum_{k=1}^{n} P_{hit}{}^{(\text{ion } k)} = \sum_{k=1}^{n} \frac{k-1}{1.2\times 10^7} = \frac{n}{2}\frac{(n-1)}{1.2\times 10^7}. \tag{4}$$

Since $n/1.2\times 10^7 \equiv \theta$ and $n \gg 1$, the total number of hits on an area of 1 μm^2 is

$$N_{hits} = \frac{1.2\times 10^7}{2}\theta^2. \tag{5}$$

At 10 eV the Co coverage is 0.19 ML, which corresponds to 2×10^5 ions/μm^2 hitting an island, which is one order of magnitude higher than the density of islands expected for thermal deposition at 300 K with a deposition rate $F = 0.002$ Å/s, i.e., $18(3)\times 10^3$ islands/μm^2. The ability of an incoming ion to fragment an island depends on the fraction of energy that can be transferred during impact. Zhou and Wadley have performed MD simulations to study the effect of 12-eV Ar^+ and Xe^+ impacts on small pyramidal Ni islands (containing ten atoms) located on a Cu(111) surface.[16] The authors explored the energy transfer of an incoming ion to the surface. For perpendicular impact at 12 eV, the Ar^+ ions transfer about 65% of their kinetic energy, whereas the heavier Xe^+ ions transfer about 80%. This energy transfer decreases with increasing angle of incidence, e.g., at 20° Ar^+ ions transfer $\pm 60\%$ of their kinetic energy and Xe^+ ions transfer $\pm 75\%$. Taking into account that ^{59}Co has a mass in between that of Ar and Xe, we can estimate the energy transfer for 10-eV impacts at 20° to be about 7 eV. Typically, the

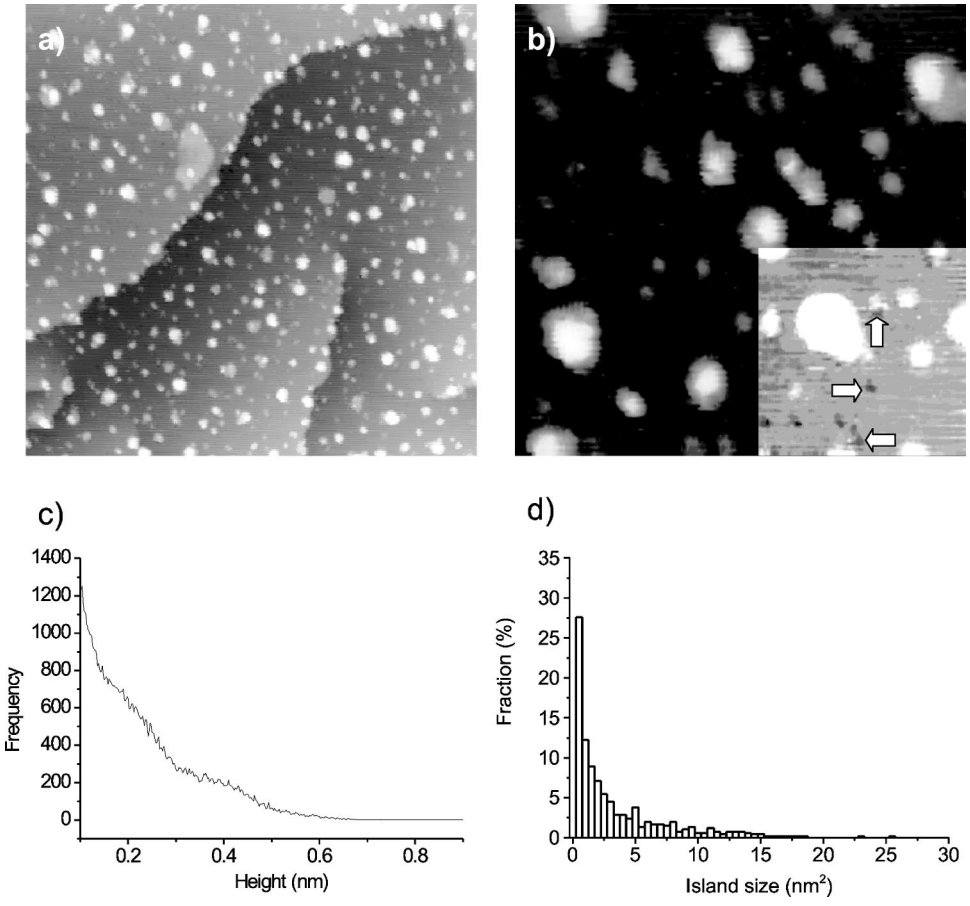

FIG. 4. An STM topograph (100×100 nm^2) of low-energy ion deposition of Co on Ag(001) at 15 eV (a), an STM topograph (30×30 nm^2) on a smaller scale with enhanced contrast on the Ag terrace level in the lower right corner, the white arrows point at some of the depressions (b), the height histogram taken from areas without Ag steps and with the terrace peak (not shown) at 0 nm (c), and the island size distribution (d).

binding energy in an island is less than 1 eV/atom.[4] Sillanpää and Koponen have investigated the effect of fragmentation for $q=0.01-0.1$ with q being the ratio between bombarding ions and deposited ions[14] [in our case $\pm 10\%$ of the incoming Co ions hit an island, see Eq. (5)]. They find that, compared to thermal deposition and for a coverage $\theta = 0.2$ ML, the island density has doubled in the case of fragmentation with $q=0.1$. These results indicate that ion impact induced island fragmentation can explain the significant increase of the island density for an increase of the deposition energy from 5 eV to 10 eV.

In Fig. 3(d) the island size distribution for 10 eV is shown. Once again the situation is completely different compared to LEID with 5 eV. Very small islands clearly dominate the morphology. This is in agreement with both an increase in the number of surface-confined Co clusters and island fragmentation. A Co cluster in the first surface layer can act as a (imperfect) pinning center and trap single Co adatoms. Once a Co adatom is trapped, a new island can start to grow. The more the Co clusters present in the first surface layer, the more new islands can form. Also fragmentation gives a decrease of the average island size. A fragmented island decreases in size and the atoms that are expelled from the island can diffuse and form new islands. Both mechanisms result in nucleation (i.e., the formation of new islands), which is no longer restricted to the early stages of deposition. As a consequence, the island size distribution will extend towards very small islands. This is confirmed by the results of Sillanpää and Koponen: with fragmentation, the number of small islands increases considerably and the average size decreases.[14] In principle, it is possible to compare the experimental island size distribution quantitatively with the scaled island size distribution obtained by Sillanpää and Koponen for fragmentation. However, the experimental island size distribution is given as a function of the surface covered by an island whereas it is needed as a function of the number of atoms contained in an island. This means that additional efforts should be made to accurately determine the relation between topography of a 3D Co island on a Ag(001) surface and the number of Co atoms contained in the island, e.g., taking into account the crystal structure of the island and island-tip convolution effects. On the other hand, a realistic model should include the probability for fragmentation with respect to ion energy, island size, impact point, etc. Therefore, a quantitative comparison between theory and experiment is currently not straightforward.

Related to the presence of Co clusters in the first surface layer, there is another mechanism that can cause an increase in island density with increasing deposition energy. The lattice parameter of fcc Co (3.55 Å) is considerably smaller than that of fcc Ag (4.09 Å). This means that a Co cluster in the first surface layer can give rise to tensile strain for both the Co and Ag atoms. This is shown schematically in Fig. 3(e). Tensile strain at the surface decreases the diffusion coefficient of adatoms.[35–37] For increasing deposition energy,

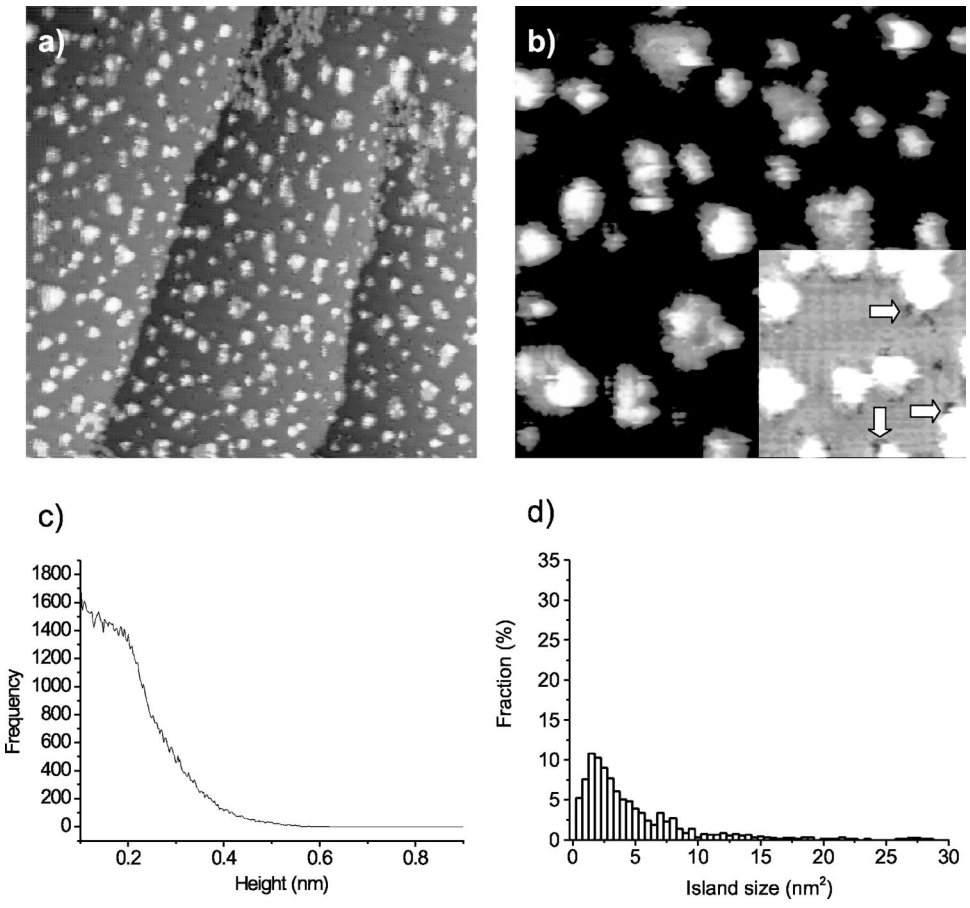

FIG. 5. An STM topograph (100×100 nm^2) of low-energy ion deposition of Co on Ag(001) at 20 eV (a), an STM topograph (30×30 nm^2) on a smaller scale with enhanced contrast on the Ag terrace level in the lower right corner, the white arrows point at some of the depressions (b), the height histogram taken from areas without Ag steps and with the terrace peak (not shown) at 0 nm (c), and the island size distribution (d).

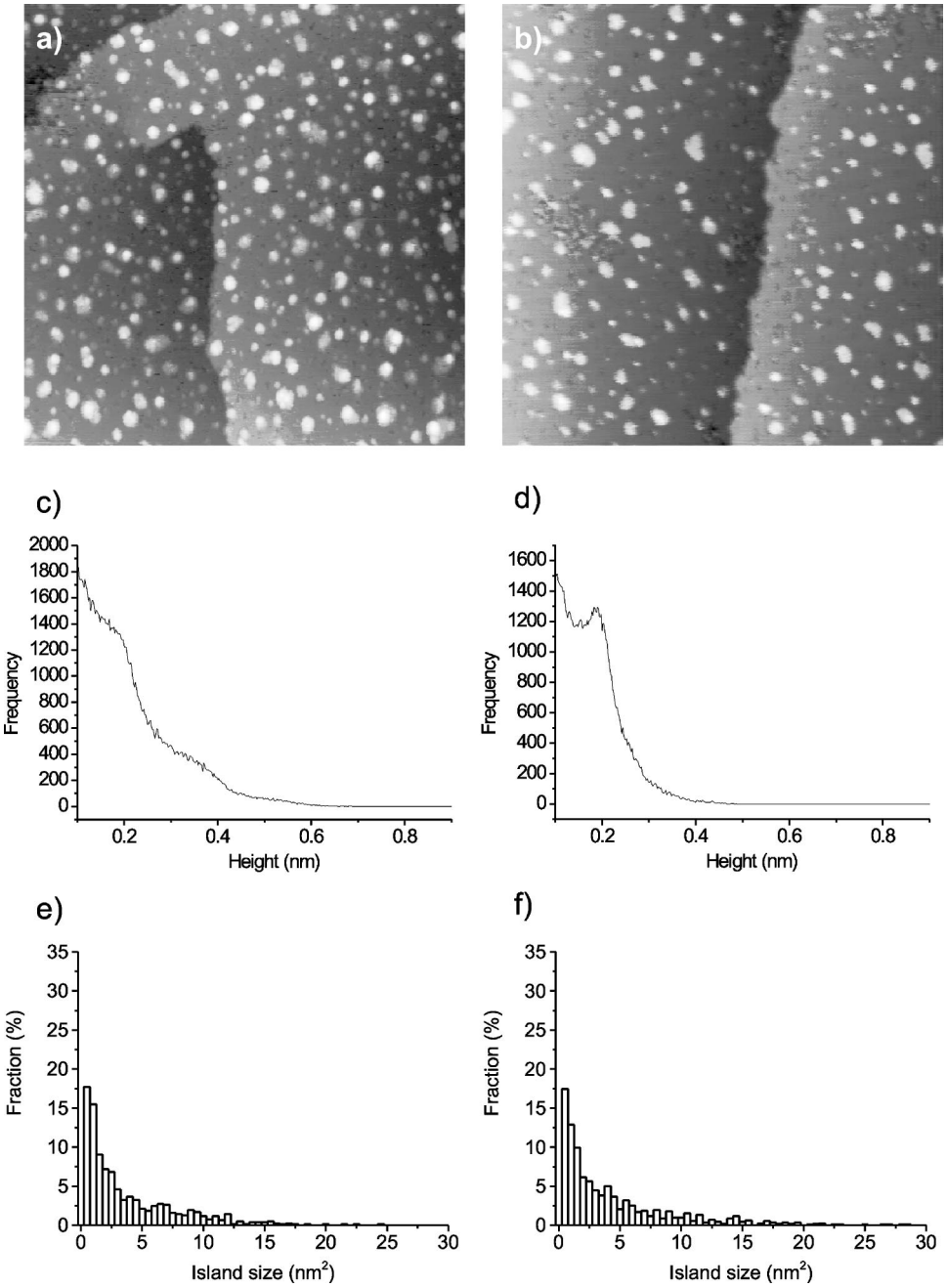

FIG. 6. An STM topograph (100×100 nm^2) of low-energy ion deposition of Co on Ag(001) at 25 eV (a) and 30 eV (b), the height histogram taken from areas without Ag steps and with the terrace peak (not shown) at 0 nm for 25 eV (c) and 30 eV (d), the island size distribution for 25 eV (e) and 30 eV (f).

the fraction of Co in the first surface layer increases and, therefore, the tensile strain increases as well. When the diffusion coefficient decreases, the island density increases [Eq. (1)]. However, based on our experimental results it is difficult to determine that to what extent this mechanism should be taken into account.

We conclude that the morphology at 10 eV is no longer comparable to thermal deposition. Ion impact induced island fragmentation and an increased density of surface-confined Co clusters result in a drastic increase of the island density and a decrease of the mean island size. The presence of Co clusters in the first surface layer might also cause an increase in tensile stress resulting in a decrease of the adatom diffusion coefficient.

C. 15 eV

In Fig. 4 an STM topograph is shown for a deposition energy of 15 eV together with its height histogram. The tail of the histogram is longer than for 10 eV indicating that the islands have grown higher. There is no Ag peak even though we expect the fraction of Ag adatoms to be comparable with or larger than 14%, which is the fraction observed for 10 eV. Looking in detail at the shape of the islands, we can distinguish small Ag patches around the higher islands [Fig. 4(b)]. The fact that we do not see a corresponding Ag peak in the height histogram is probably due to the presence of many small, low islands. In the histogram, such islands contribute considerably to heights just above the terrace, i.e., between 0 and 0.2 nm. As a consequence, there is no longer a distinct

difference between the terrace peak and the islands on top of the terrace. This is clear from the slope of the histogram at 0.1 nm: it is much steeper than in the case of 5 eV. Whether these small islands consist of Co or Ag or both is not clear. In principle, we expect that Ag islands are large (see Fig. 1.17 in Ref. 23) because of the high mobility. In the case of LEID, this argument no longer holds due to fragmentation and the presence of Co pinning centers. As a consequence, it is difficult to determine the relative fraction of Co and Ag from the histogram. Assuming that the fraction of Ag is around 20% we find a coverage of 0.15 ML of Co and 0.05 ML of Ag. This is an estimation based on our MD calculations and on the fact that the fraction of Co in the first surface layer increases with increasing energy.

Beside the analysis of the histogram, the island density was determined: $45(10)\times10^3$ islands/μm^2. This is higher than what is expected for thermal deposition, indicating that fragmentation occurs and that Co pinning centers are present in the first ML. The density is lower though, than in the case of 10 eV. With increasing energy, fragmentation will become more efficient. In addition, the number of pinning centers increases for increasing energy, since $\tilde{F}$ increases (Sec. III A). In the lower right corner of Fig. 4(b) the contrast on the Ag terrace level is enhanced. We can clearly see the depressions corresponding to submerged Co clusters. The total coverage from islands on top of the surface (Co + Ag) for 10 and 15 eV is comparable, but the Co coverage is somewhat lower in the case of 15 eV (0.19 ML for 10 eV vs 0.15 ML for 15 eV). Since new islands are formed at any stage of deposition (due to fragmentation and the presence of pinning centers), a lower coverage implies a lower island density. On the other hand, for deposition energies higher than 10 eV we never observed a higher island density (than that for 10 eV), even when the Co coverage is higher. Therefore, the decrease in island density cannot completely be explained by differences in coverage. The only remaining explanation for this behavior is the fact that ion induced island dissociation occurs: due to the energetic impact of ions on an island, the bonds that hold the island together are broken and all Co atoms become adatoms again. These Co adatoms can attach to an existing island or form a new island. In the former case, the island density is decreased, in the latter case it remains unchanged.

What is the energy needed to dissociate an island? Stoltze and Nørskov have performed MD calculations for Cu on Cu(111) and determined the binding energy for clusters with 2–12 atoms.[4] For each extra atom the binding energy increases by 0.6–0.9 eV. For a cluster of 12 atoms they obtained a binding energy of $\pm$8 eV. Stroscio and Pierce found a bond energy of $\pm$0.5 eV for Fe on Fe(001).[38] On a (001) surface, islands containing 9, 16, or 25 atoms can have the compact shape of a square. With 0.5 eV per bond this gives a binding energy of 6, 12, and 20 eV respectively. This indicates that for the energy range studied in this work (5–30 eV), only small islands are possibly dissociated: with a lattice parameter corresponding to that for Ag (i.e., $a_0 = 4.09$ Å) a ML high island containing 25 atoms corresponds to an area of 2 nm^2. Furthermore, islands can only be dissociated when there is a sufficient transfer of kinetic energy from the incoming ion to the atoms of the island. As mentioned in Sec. III B, Zhou and Wadley have performed MD simulations to study the effect of Ar^+ and Xe^+ impacts on small Ni islands on a Cu(111) surface.[16] These islands were separated by only a few lattice parameters. For an impact energy of 12 eV, they found that most of the islands were reduced to ML height at incident angles ranging from 0° to 70° off normal. In addition, the island density was always reduced compared to the initial island density before ion bombardment. For a 15-eV $^{59}Co^+$ ion the energy transfer for an impact angle of 20° can be estimated at 9 eV. This is sufficient to dissociate small islands containing less than ten atoms.

TABLE I. The island density as a function of deposition energy.

Deposition energy (eV)	Island density (10^3 islands/μm^2)
5	26(4)
10	87(20)
15	45(10)
20	40(7)
25	49(13)
30	40(11)

For a deposition energy of 15 eV, there is a large fraction of small islands after deposition (see below): 49% is smaller than 1.5 nm^2. Such islands contain less than 18 atoms. The Co coverage on top of the surface is 0.15 ML. According to Eq. (5), 1.35×10^5 islands per μm^2 are hit after deposition. This is about three times the experimentally observed island density (i.e., 42×10^3 islands/μm^2). Since the number of ion impacts on small islands is sufficiently large, fragmentation and dissociation are expected to affect the island density significantly. Fragmentation and dissociation have an opposite effect on the island density, the former gives an increase and the latter a decrease of n_x. However, more energy is needed to dissociate an island because in the case of fragmentation less bonds are broken. This explains why at 10 eV the island density is higher than at 15 eV. At 10 eV, fragmentation occurs already whereas the deposition energy is too low to cause a considerable number of dissociations. At 15 eV, dissociation also becomes important, which results in a decrease of the island density compared to 10 eV.

In conclusion, the morphology at 15 eV is determined by the balance between mechanisms with an opposite effect on the island density. On the one hand, fragmentation and an increasing number of pinning centers in the first surface layer cause an increase of the island density for increasing energy. On the other hand, island dissociation causes a decrease in the island density for increasing deposition energy.

In Fig. 4(d) the island size distribution for 15 eV is shown. The large fraction of small islands (<1.5 nm^2) indicates that nucleation is still determined by fragmentation and the presence of pinning centers. Compared to 10 eV the fraction of small islands is lower. This is in agreement with a higher efficiency of island dissociation at 15 eV: large islands

can grow at the expense of small islands (i.e., only small islands can dissociate at this low energy).

Finally at 15 eV, there is again preferential nucleation on the upper sides of the Ag step edges [Fig. 4(a)]. Due to dissociation of small islands, Co adatoms become available again for growth, which results in a more *thermal-like* morphology. This means that also step decoration becomes possible again. The number of nucleation sites at a step edge is smaller than in the case of 5 eV indicating that the nucleation behavior is not completely thermal and pinning centers still play an important role. The latter is also clear from the island size distribution.

D. 20 eV

An STM image for 20 eV is shown in Fig. 5 together with its height histogram. As in the case of 15 eV there is no well-defined Ag peak, though there is a bump at 0.2 nm, confirming the presence of Ag. In Fig. 5(b) a detailed STM image is shown: many islands are surrounded by a ML patch. According to MD calculations, from 20 eV onwards, vacancies can be produced.[24] When vacancies are created, more than one Ag atom becomes an adatom for each Co atom ending up in the first surface layer. A fraction of $\pm 40\%$ Ag is expected on top of the surface. Based on the height histogram and the STM images we believe that this is an overestimation since this would give a large peak at 0.2 nm in the histogram. Taking a fraction of 25% Ag we find a Co coverage of 0.21 ML. This is 5% higher than what we took for 20 eV in order to make an estimate of the Co and Ag coverage.

An island density of $40(7)\times 10^3$ islands/μm^2 is obtained, which is comparable to 15 eV. The observation of similar depressions in the terraces confirms the presence of surface-confined Co clusters [inset of Fig. 5(b)]. The size distribution for 20 eV is somewhat different than for 15 eV [Fig. 5(d)]. We believe that the average island size has increased due to larger Ag patches around the Co islands compared to 15 eV. Larger patches lead to an apparent increase in the Co islands. This difference in island size distribution is related to the subtle balance between fragmentation and pinning on the one hand and dissociation on the other hand. There are several indications that these are the primary mechanisms that determine the morphology: (1) there is experimental evidence of the presence of Co pinning centers [Fig. 5(b)]; (2) the island density is higher than what is expected for thermal deposition (in agreement with fragmentation), but lower than for 10 eV (in agreement with dissociation); (3) when Ag patches are subtracted form the STM images, the island size distribution is shifted to smaller islands.

E. 25 eV

In Fig. 6(a) an STM image is shown for a deposition energy of 25 eV. Due to the presence of small islands there is no Ag peak at 0.2 nm in the histogram but only a bump. This was also the case for 20 eV. It is again difficult to determine the relative fractions of Co and Ag. In order to give an estimate of the coverage, the fraction of Co in the first surface layer is increased by 5% for every 5 eV from 15 eV onwards. Supposing that 30% of Co ends up in the first surface layer, a coverage of 0.17 ML of Co and 0.08 ML of Ag is found. We obtain an island density of $49(13)\times 10^3$ islands/μm^2.

In Fig. 6(e), the island size distribution is shown. There is a large fraction of small islands but this fraction is lower than in the case of 10 eV. These observations can again be explained as a combination of fragmentation, pinning, and dissociation. The island density is higher than what is expected for thermal deposition but lower than for 10 eV. Again we observe depressions corresponding to surface-confined Co clusters (not shown). The island size distribution is similar to those of 10 and 15 eV. This is also the case for 30 eV as we will see in the following section.

F. 30 eV

At 30 eV [Fig. 6(b)] there is again a Ag peak in the histogram [Fig. 6(d)]. There is a considerable number of small islands and consequently the Ag fraction, obtained by using the method of analysis used also for the codeposition experiments, is underestimated. With a fraction of 35% of Co ending up in the first surface layer we find a coverage of 0.11 ML of Co and 0.05 ML of Ag. The tail of the histogram resembles that for 10 eV implying low islands. The island density is $40(11)\times 10^3$ islands/μm^2. The island size distribution is shown in Fig. 6(f). There is a large fraction of small islands. However, this fraction is again smaller than in the case of 10 eV. The morphology at 30 eV is very similar to 25 eV and can also be explained in terms of fragmentation, pinning, and dissociation. Also for 30 eV we observe depressions in the terraces indicating that there are Co clusters in the first surface layer. The coverage (Co + Ag) is somewhat lower than in the case of 25 eV, which might explain the lower island density observed at 30 eV.

IV. CONCLUSION

We have investigated the influence of the deposition energy with respect to nucleation and growth of Co on Ag(001). Co was deposited by low-energy ion deposition with an energy between 5 and 30 eV. Table I gives an overview of the island densities for the various energies. For an energy of 5 eV, the morphology of a submonolayer Co film is similar to thermal deposition with an additional fraction of Ag present on the surface ($\pm 10\%$ of the Co coverage). At 10 eV there is a drastic increase of the island density combined with a decrease of the island size and height. This is explained in terms of ion impact induced island fragmentation and an increase in the number of surface-confined Co clusters. The presence of depressions in the vicinity of the islands indicates that such Co clusters act as pinning centers for Co adatoms during the nucleation. The morphology for deposition energies between 15 and 30 eV is characterized by an island density that is higher than the island density for thermal deposition but lower than for 10 eV. The only mechanism causing a decrease of the island density for increasing ion energy is ion impact induced island dissociation. As in the case of 10 eV, for 15 to 30 eV depositions there is a large fraction of small islands and depressions present in the terrace. This indicates that fragmentation and pinning

still play an important role at these higher deposition energies, resulting in an island density larger than that for thermal deposition.

Our experimental results indicate that at least three mechanisms influence the morphology of a LEID grown film: ion impact induced island fragmentation, pinning at surface-confined clusters, and ion impact induced island dissociation. In addition, as mentioned in Sec. III B, the tensile strain due to the presence of Co clusters in the first surface layer possibly causes an increase in the island density for increasing deposition energy. We have no indications that either transient mobility, enhanced mobility due to direct or indirect ion impact, or adatom sputtering give rise to a significant change in the morphology of the film. Based on codeposition experiments of Co and Ag on Ag(001), we can rule out the possibility that Co adatoms nucleate at ion impact induced Ag adatoms (Sec. III A).

This work was supported by the Belgian Fund for Scientific Research of Flanders (FWO), the Concerted Action (GAO), and the Inter-University Attraction Pole (IUAP P4/10).

*Electronic address: bart.degroote@fys.kuleuven.ac.be

[1] J. W. Rabalais, A. H. Al-Bayati, K. J. Boyd, D. Marton, J. Kulik, Z. Zhang, and W. K. Chu, Phys. Rev. B **53**, 10 781 (1996).
[2] D. Sanders and A. DePristo, Surf. Sci. **254**, 341 (1991).
[3] D. Sanders, D. Halstead, and A. DePristo, J. Vac. Sci. Technol. A **10**, 1986 (1992).
[4] P. Stoltze and J. K. Nørskov, Phys. Rev. B **48**, 5607 (1993).
[5] C. Laurens, Ph.D. thesis, Rijksuniversiteit, Groningen, 1997.
[6] B. W. Dodson, Phys. Rev. B **36**, 1068 (1987).
[7] G. Carter, Vacuum **55**, 235 (1999).
[8] M. Ghaly, K. Nordlund, and R. Averback, Philos. Mag. A **79**, 795 (1999).
[9] M. Morgenstern, T. Michely, and G. Comsa, Philos. Mag. A **79**, 775 (1999).
[10] X. Zhou and H. Wadley, Surf. Sci. **431**, 42 (1999).
[11] S. Esch, M. Bott, T. Michely, and G. Comsa, Appl. Phys. Lett. **67**, 3209 (1995).
[12] S. Esch, M. Breeman, M. Morgenstern, T. Michely, and G. Comsa, Surf. Sci. **365**, 187 (1996).
[13] M. Kalff, M. Breeman, N. Morgenstern, T. Michely, and G. Comsa, Appl. Phys. Lett. **70**, 182 (1997).
[14] J. Sillanpää and I. Koponen, Nucl. Instrum. Methods Phys. Res. B **142**, 67 (1998).
[15] E. Chason and B. Kellerman, Nucl. Instrum. Methods Phys. Res. B **127/128**, 225 (1997).
[16] X. Zhou and H. Wadley, Surf. Sci. **487**, 159 (2001).
[17] G. Rosenfeld, N. Lipkin, W. Wulfhekel, J. Kliewer, K. Morgenstern, B. Poelsema, and G. Comsa, Appl. Phys. A: Mater. Sci. Process. **A61**, 455 (1995).
[18] J. Sprague and C. Gilmore, Thin Solid Films **272**, 244 (1996).
[19] S. Todorov, H. Bu, K. Boyd, J. Rabalais, C. Gilmore, and J. Sprague, Surf. Sci. **429**, 63 (1999).
[20] M. Weiss, M. Lu, P. Van der Heide, S. Lee, E. Ada, H. Lee, and J. Rabalais, J. Chem. Phys. **113**, 5058 (2000).
[21] W. Wulfhekel, I. Beckmann, G. Rosenfeld, B. Poelsema, and G. Comsa, Surf. Sci. **395**, 168 (1998).
[22] J. Dekoster, B. Degroote, H. Pattyn, G. Langouche, A. Vantomme, and S. Degroote, Appl. Phys. Lett. **75**, 938 (1999).
[23] B. Degroote, Ph.D. thesis, K.U. Leuven (2001), available in the pdf format at http://www.fys.kuleuven.ac.be/iks/nvsf/nvsf.html.
[24] B. Degroote, A. Vantomme, H. Pattyn, K. Vanormelingen, and M. Hou, following paper, Phys. Rev. B **65**, 195402 (2002).
[25] B. Degroote, J. Dekoster, and G. Langouche, Surf. Sci. **452**, 172 (2000). (In this reference we reported a value of $\Delta E = 0.6(2)$ eV for terrace diffusion. However, in the analysis ν_0 was not $10^{12\pm1}$ Hz but was taken as a fitting parameter giving $\nu_0 = 10^{10\pm4}$ Hz. This illustrates how ΔE is very much dependent on the value of the diffusivity. This is discussed in detail in Ref. 23.)
[26] H. Brune, Surf. Sci. Rep. **31**, 121 (1998).
[27] J. de la Figuera, J. E. Prieto, C. Ocal, and R. Miranda, Phys. Rev. B **47**, 13 043 (1993).
[28] L. Gomez, C. Slutzky, J. Ferron, J. de la Figuera, J. Camarero, A. L. Vazquez de Parga, J. J. de Miguel, and R. Miranda, Phys. Rev. Lett. **84**, 4397 (2000).
[29] A. Brodde and H. Neddermeyer, Ultramicroscopy **42-44**, 556 (1992).
[30] M. Klaua, H. Höche, H. Jenniches, J. Barthel, and J. Kirschner, Surf. Sci. **381**, 106 (1997).
[31] J. Venables, G. Spiller, and M. Hanbrücken, Rep. Prog. Phys. **47**, 399 (1984).
[32] M. F. Roşu, C. R. Laurens, A. Falepin, M. A. James, M. H. Langelaar, F. Pleiter, O. C. Rogojanu, and L. Niesen, Phys. Rev. Lett. **81**, 4680 (1998).
[33] M. Langelaar, M. Breeman, and D. Boerma, Surf. Sci. **352-354**, 597 (1996).
[34] G. L. Kellogg, Phys. Rev. Lett. **73**, 1833 (1994).
[35] H. Brune, K. Bromann, H. Roder, K. Kern, J. Jacobsen, P. Stoltze, K. Jacobsen, and J. Nørskov, Phys. Rev. B **52**, R14 380 (1995).
[36] M. Schroeder and D. Wolf, Surf. Sci. **375**, 129 (1997).
[37] R. Mattsson and H. Metiu, J. Chem. Phys. **113**, 10 323 (2000).
[38] J. A. Stroscio and D. T. Pierce, Phys. Rev. B **49**, 8522 (1994).